Coherent population trapping under periodic polarization modulation: Appearance of the CPT doublet

M. Huang and J. C. Camparo

Physical Sciences Laboratories, The Aerospace Corporation, P.O. Box 92957, Los Angeles, California 90009, USA

In order to understand how stochastic processes might enter and influence coherent atomic dynamics, we have studied the behavior of a Λ system under periodic polarization modulation. Polarization, in addition to amplitude and phase, is a defining feature of a classical vector field. However, to date, there has been little study concerning the response of quantum systems to temporal variations in polarization, even though some lasers are known to exhibit stochastic polarization fluctuations. In our work, we square-wave modulate the polarization of a laser that induces coherent-population trapping (CPT) in ^{87}Rb. At low-modulation frequencies, we find that the amplitude of the CPT resonance increases with modulation frequency because the polarization variations limit the number of atoms confined to the system's trapping state. Surprisingly, at higher-modulation frequencies, we find that the CPT resonance splits into a doublet. We have developed an analytical theory of CPT in the presence of polarization modulation that captures the primary features of our experimental findings and shows that the doublet is a consequence of ground-state coherence modulation in the Λ system. The present results lay a foundation for understanding how more complicated (i.e., stochastic) temporal variations in laser polarization could influence Λ-system dynamics.

I. INTRODUCTION

The phenomenon of coherent-population trapping (CPT) [1,2], which has led to the development of chip-scale atomic clocks [3,4], is routinely conceptualized in terms of a three-level system interacting with a bichromatic field [5]. Briefly, as illustrated in Fig. 1 for the ^{87}Rb system, when the bichromatic field resonantly couples two ground-state eigenfunctions to a common excited state, destructive interference between the two excitation pathways can take place. This interference effectively turns off the atom's absorption cross section [6] so that, for a vapor of atoms, there is a resonant increase in the light intensity transmitted by the vapor. Importantly for atomic-clock applications, the linewidth of this CPT signal is not defined by any optical dephasing rate but rather by the dephasing time of the ground-state coherence, which, in the case of the alkali metals, can be 4 to 5 orders of magnitude longer than the optical dephasing time.

As illustrated in Fig. 1, realization of the CPT phenomenon for the alkali-metal 0-0 hyperfine states requires a circularly polarized field [7] so that (for example) the $|F = 1, m_F = 0\rangle$ and $|F = 2, m_F = 0\rangle$ ground-state eigenfunctions only couple to the $|F' = 2, m_F = +1\rangle$ excited state. Of course, the absorption of circularly polarized light transfers angular momentum from the light field to the atomic system, and as a consequence, the atomic vapor develops a nonzero electronic-spin polarization $\langle S_z \rangle$ [8–10]. Electronic-spin polarization plays the role of a *noncoherent* dark state (or equivalently, a trapping state), which reduces the alkali-vapor density contributing to the *coherent* dark state (i.e., the dark state associated with CPT) and thereby reduces the amplitude of the CPT signal [11]. To overcome this problem, various research groups have devised more sophisticated techniques for CPT signal generation: push-pull optical pumping [12], lin $\perp$ lin excitation [13], and phase-delayed bichromatic fields [14,15]. The common thread to these techniques is that the circular polarization of

the bichromatic field is modulated between right-circularly and left-circularly polarized light at a microwave frequency. As a consequence, while no net angular momentum is transferred to the vapor (i.e., the noncoherent dark state is eliminated), the coherent dark state is preserved.

In the present paper, our attention also is focused on issues of polarization modulation and the CPT phenomenon. However, although we are certainly interested in polarization modulation as a means to increase the amplitude of CPT signals, our primary interest is directed toward a different question: How does low-frequency polarization modulation (i.e., $f_m \leqslant 10^6$ Hz) affect CPT line shapes? This specific question is part of a much broader research area aimed at elucidating the stochastic-field–atom interaction [16] and is important in CPT since laser polarization fluctuations may represent a novel pathway for stochastic fields to affect the signal-to-noise ratio of chip-scale atomic clocks.

In the following section, we discuss our experimental arrangement and our findings. In particular, we have discovered that a CPT resonance will split into a doublet when the polarization modulation frequency exceeds the 0-0 dephasing rate. In Sec. III, we present an analytical theory of the splitting where the motivation is to uncover the fundamental characteristics of the atomic dynamics that give rise to the splitting. Finally, in Sec. IV, we provide a brief discussion of the implications of our findings for the stochastic-field–atom interaction problem.

II. EXPERIMENT

Our experimental arrangement is illustrated in Fig. 2. To generate the Λ-system coherence, we employed a cleaved-facet Fabry-Pérot diode laser [17], which does not suffer the intrinsic polarization fluctuations sometimes observed in vertical-cavity surface-emitting lasers (VCSELs) [18]. The laser light then passed through an electro-optic modulator,
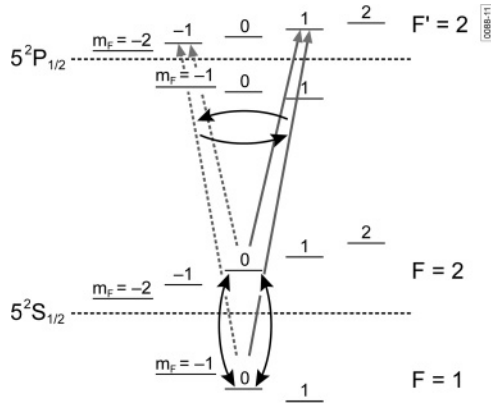
FIG. 1. In the typical CPT experiment with ^{87}Rb, two modes of a laser couple the atom's two $5\,^2S_{1/2}$ ($m_F = 0$) ground-state sublevels to the same excited state; here, the common excited state is the $5\,^2P_{1/2}\,|F' = 2, m_F = +1\rangle$ state. The simultaneous coupling creates a coherence in the ground state, indicated by the double-headed arrows, and it is this coherence that is at the heart of the CPT phenomenon. If the laser polarization fluctuates, then the common excited state momentarily changes to $|F' = 2, m_F = -1\rangle$, and this affects the ground-state coherence.

which placed sidebands on the laser at $\pm\Delta_s \cong \pm\omega_{\text{hfs}}/2$ with a single-sideband-to-carrier intensity ratio (I_s/I_c) of 0.17; here, ω_{hfs} is the ground-state hyperfine transition frequency (i.e., 6834.7 MHz for ^{87}Rb). The beam diameter was 0.4 cm so that the intensity of a single sideband I_s was $\sim$250 μW/cm^2. [Although not shown, the light also passed through a neutral-density (ND) filter, allowing variation in the laser intensity.] The modulated and linearly polarized field then passed through a ferroelectric liquid-crystal polarization rotator (manufactured by Micron Technology, Inc.), which has a bandwidth of 10 kHz, and changes the field's linear polarization by $90°$ depending on an applied voltage. Following this, the field passed through a quarter-wave plate, creating right- or

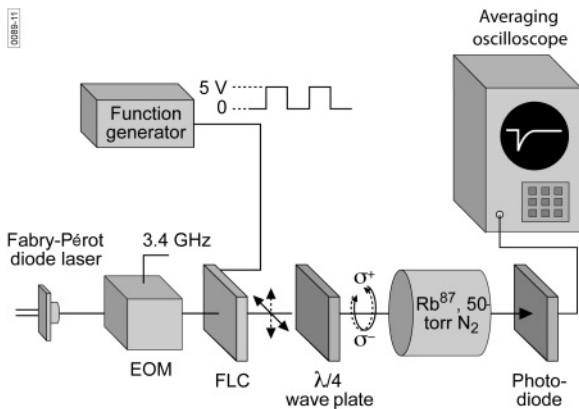
FIG. 2. Block diagram of our experimental arrangement. The Rb cell was maintained at a temperature of 47 $°$C, corresponding to an alkali-metal density of $\sim$10^{11} cm^{-3}, and the Rb atoms were contained with a 50-torr N$_2$ buffer gas. The laser light passed through an electro-optic modulator that placed sidebands on the laser at $\sim$3.4 GHz. Additionally, although not shown, the light passed through a ND filter. In our experiments, the single sideband-to-carrier power ratio was 0.17.

left-circularly polarized light and then passed into a resonance cell containing isotopically enriched ^{87}Rb and 50 torr of N$_2$ as a buffer gas; using N$_2$, the dominant relaxation mechanism in our system was electron-spin randomization (also known as S damping) [10]. Pressure broadening of the optical transitions by N$_2$ also ensured that the excited-state hyperfine structure was unresolved [19]. Our Pyrex resonance cell was 3.9-cm long with a diameter of 2.2 cm and was maintained at 47 $°$C with braided heating wire wrapped around the cell body; the intrinsic attenuation coefficient of the vapor κ_o was 1.0: $I(L) = I_o e^{-\kappa_o} = I_o e^{-[\text{Rb}]\sigma L}$ with I_o defined as $I_s \times 10^{-\text{ND}}$. The resonance cell was located in a set of three mutually perpendicular Helmholtz coils with a diameter of 66 cm [20]: Two pairs cancelled out the Earth's magnetic field, while the third provided a quantization axis for the atoms along the laser beam's propagation direction (i.e., $B_z = 0.5$ G).

Figure 3(a) shows an example of our CPT line shape in the absence of polarization modulation for a relative light intensity I_o/I_s of 0.13. The solid line through the data is a Lorentzian fit, which has a HWHM $\Delta\nu_{1/2}$ of 697 s^{-1} (i.e., 111 Hz). Figure 3(b) shows our measured values of $\Delta\nu_{1/2}$ as a function of relative light intensity. From these data, we inferred that our intrinsic dephasing rate γ_2 was 319 s^{-1} and
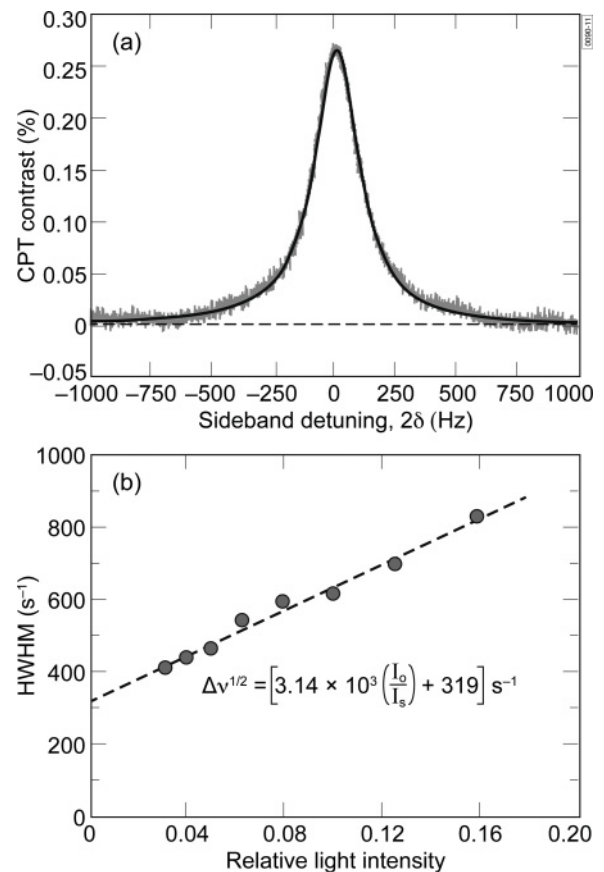

FIG. 3. (a) An example of our CPT line shapes in the absence of polarization modulation; the data were taken with a relative light intensity I_o/I_s of 0.13, and the solid line through the data is a Lorentzian least-squares fit. (b) Plot of the half width at half maximum (HWHM) $\Delta\nu_{1/2}$ from the Lorentzian least-squares fits as a function of relative light intensity; the data indicate that our intrinsic dephasing rate γ_2 is 319 s^{-1}.

that the optical excitation rate $R \equiv \Omega^2/\Gamma$ was given by $R = 3.14 \times 10^3(I_o/I_s)$ s^{-1}; here, Ω is the optical Rabi frequency, and Γ is the excited-state decay rate. Since we employ 50 torr of N$_2$ as a buffer gas in our experiments, Γ is affected by the rate of quenching collisions Γ_Q: $\Gamma = A + \Gamma_Q$, where A is the Einstein-A coefficient for the D_1 Rb transition (i.e., 3.65×10^7 s^{-1} [21]). Taking the quenching cross section for the $5\,^2P_{1/2}$ state as 5.8×10^{-15} cm^2 [22], we have $\Gamma = 5.7 \times 10^8$ s^{-1}. If we now define the saturation intensity I_{sat} through the relation $n_e = 0.5(I/I_{\text{sat}})/[1 + I/I_{\text{sat}}] = 0.5(R/\Gamma)/[1 + R/\Gamma]$, where n_e is the relative excited-state density, then, at our full sideband light intensity, we have $I_s/I_{\text{sat}} = 5.5 \times 10^{-6}$. The light intensity that maximized our CPT contrast in the absence of polarization modulation I_m corresponded to $\text{I}_m/I_s = 0.079$ or equivalently $I_m/I_{\text{sat}} = 4.4 \times 10^{-7}$.

In a previous paper, we examined the transient response of this atomic system to a *step change* in laser polarization [23]. We found that the simplest semiempirical theory capable of capturing the dominant features of the transient dynamics corresponded to a seven-parameter model of the attenuation coefficient $\kappa(t)$,

$$\kappa(t) = A_f e^{-\gamma_f t} + A_s e^{-\gamma_s t} - A_2 e^{-\gamma_2 t} \sin(2\delta t). \quad (1)$$

Although a seven-parameter model may seem overly generous, we note that this is actually the minimum number of parameters that are required based on more rigorous theoretical considerations. In Eq. (1), the first two terms on the right-hand side correspond to a biexponential transient in $\langle S_z \rangle$ arising from electron-spin randomizing collisions with N$_2$ [8] (i.e., a fast exponential and a slow exponential that derive from the nucleus's ability to act as a reservoir of angular momentum). In effect, these two terms correspond to bulk motion of the population density from one side of a ground-state Zeeman multiplet to the other. The third term on the right-hand side corresponds to a nutationlike transient: As the polarization suddenly changes, there is a discontinuity in the 0-0 coherence, which oscillates at $2\delta \equiv 2\Delta_s - \omega_{\text{hfs}}$ and returns to equilibrium at the dephasing rate.

At the light intensity that maximized the CPT contrast, our previous results (in a 30-torr N$_2$ cell) yielded $\gamma_f \cong 100$ s^{-1} and $\gamma_s \cong 30$ s^{-1}, where it is to be noted that these terms are longitudinal relaxation rates for $\langle S_z \rangle$. Furthermore, we found that the transients were dominated by the A_f and A_s terms (i.e., the bulk motion of population density among the Zeeman sublevels), and for all light intensities the $\langle S_z \rangle$ bulk-motion transient was six times larger than the actual CPT resonance, implying that even short-lived laser polarization variations can have a significant influence on CPT signal-to-noise ratios.

Notwithstanding the biexponential nature of the $\langle S_z \rangle$ relaxation, in order to better elucidate the underlying physics of polarization modulation in what follows, we will approximate the electron-spin randomizing mechanism of $\langle S_z \rangle$ with a *uniform* relaxation rate γ_1. After accounting for a 5/3 rate increase due to our larger N$_2$ density, we, therefore, anticipate requiring a γ_1 value in the range of 50–110 s^{-1}. In other words, employing uniform $\langle S_z \rangle$ relaxation as a surrogate for the two terms on the right-hand side of Eq. (1), we expect the requisite value of γ_1 for our theory to lie somewhere between γ_s and $(\gamma_s + \gamma_f)/2$.

Since many random processes can be modeled as an incoherent Fourier series [24], our motivation in the present paper was to lay the foundations for an *empirical* understanding of Λ systems in the presence of stochastic-polarization fields [25], and this was to be accomplished by studying the CPT resonance in the presence of square-wave laser polarization modulation. For a given value of the square-wave modulation frequency ω_m, we slowly swept the sideband spacing through the CPT resonance and recorded the change in the transmitted light intensity. The sweep of the sideband spacing was repeated at a frequency ω_{rep} so that the CPT line shapes could be averaged. Of course, as suggested by Eq. (1), every time the polarization changes at $2\omega_m$, we must expect a large transient in the transmitted light intensity. Although such transients will be important for understanding the CPT noise spectrum in the full stochastic-field–atom interaction problem, in the present work, we were not primarily interested in those transients. Rather, we were interested in understanding how polarization modulation might modify the underlying CPT line shape. Consequently, we chose ω_m to be incommensurate with ω_{rep}. In that way, the starting phase of the square-wave modulation for different frequency sweeps through the CPT line shape would be quasirandom, and therefore the exponential transients following each polarization change would eventually average to zero.

Figure 4 illustrates several CPT line shapes for different values of the modulation frequency with $I_o/I_s = 0.45$. At low-modulation frequencies $\omega_m \sim 19$ s^{-1} (i.e., 3 Hz), we see the standard CPT resonance. The noise on the CPT signal is not noise at all but a residual of the exponential transients in the transmitted light intensity following each polarization change. At intermediate modulation frequencies $\omega_m \sim 188$ s^{-1} (i.e., 30 Hz), we see an increase in the CPT signal amplitude. This was expected based on our previous paper and that of Jau *et al.* [12], since these modulation frequencies exceed the longitudinal relaxation rate of electronic-spin polarization γ_1. In other words, at these modulation frequencies the light field is unable to efficiently transfer angular momentum orientation to the vapor, and so the number of atoms in the so-called trapping state is reduced. Interestingly, however, as ω_m exceeds the 0-0 coherence dephasing rate, the CPT line shape no longer simply increases in amplitude; rather, it splits into a doublet with the separation between the two CPT resonances increasing with the modulation frequency. This is shown more quantitatively in Fig. 5 where we have plotted the center frequency of each doublet component $\omega_\pm$ as a function of the modulation frequency. In the figure, the two straight lines correspond to $\omega_+ = +\omega_m$ and $\omega_- = -\omega_m$. Finally, Fig. 6 shows the CPT contrast as a function of modulation frequency. For $\omega_m < \gamma_2$, the CPT contrast increases with modulation frequency; however, for $\omega_m > \gamma_2$, the splitting causes a decrease in the CPT contrast, which appears to asymptote to a constant value at very large modulation frequencies.

III. THEORY

In this section, we want to develop a closed-form expression for the CPT line shape in the presence of square-wave polarization modulation. Certainly, *multilevel* density matrix equations for the Rb atom in the presence of any modulated quantity
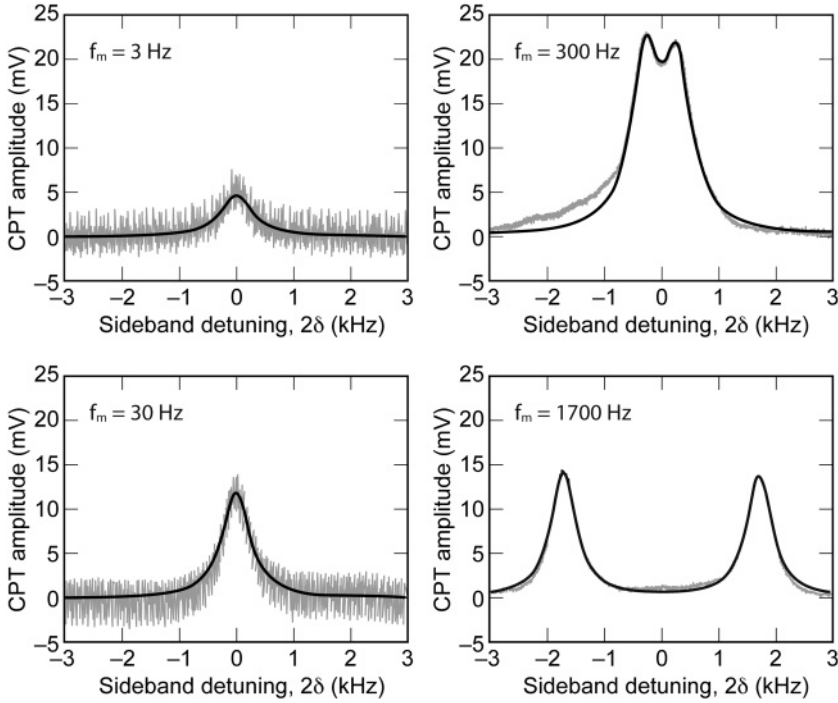
FIG. 4. As illustrated by the data in this figure, taken with $I_o/I_s = 0.45$, at low-modulation frequencies we obtain the standard CPT resonance. At intermediate frequencies (i.e., 30 Hz), the CPT amplitude increases since atoms do not have time to become trapped in a non-CPT participating atomic state. At the highest-modulation frequencies (i.e., $f_m > 300$ Hz), our CPT resonance splits into a doublet. The solid lines correspond to least-squares Lorentzian (or double Lorentzian) fits to the data, where we only fit the data for normalized values of the CPT line shape greater than 0.5.

can be derived and then solved numerically. However, while the results of such numerical computations are valuable and can be compared to the experiment, they often make it difficult to uncover the primary dynamical elements responsible for the atomic system's behavior. Here, our motivation is to understand the underlying physical origin of the CPT-doublet's and the CPT-contrast's dependences on modulation frequency. Consequently, our goal in this section is to develop a relatively simple density-matrix description of the phenomenon that leads to closed-form expressions.
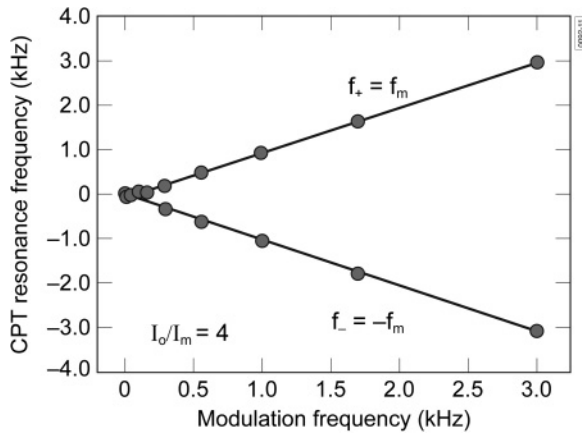

FIG. 5. The frequency of each doublet component is plotted as a function of the modulation frequency. For these results, the laser intensity was four times larger than that yielding the maximum CPT contrast in the absence of polarization modulation (i.e., $I_o/I_m = 4$). Note that the doublet splitting equals $2f_m$. Although it may appear that the splitting suddenly appears at $f_m \cong 250$ Hz, it should be recognized that the CPT resonance is broadening before it splits so that the sudden appearance of a doublet in the graph is simply due to our experimental inability to resolve the splitting at low-modulation frequencies.

In our experiments, the alkali-metal atoms are maintained with a relatively large buffer gas density so that the excited-state hyperfine structure is unresolved. The optical absorption cross section σ, therefore, can be written as [26]

$$\sigma = \sigma_o(1 - 2\vec{s} \cdot \langle \vec{S} \rangle), \qquad (2)$$

where $\vec{s}$ is the photon-spin vector (i.e., $m_s \equiv \xi = +1$ for right-circularly polarized light and $\xi = -1$ for left-circularly polarized light as projected onto the field's propagation direction) and $\langle \vec{S} \rangle$ is the expectation value of the alkali-metal ground-state electron-spin polarization. In the present situation, where the laser's propagation direction is parallel
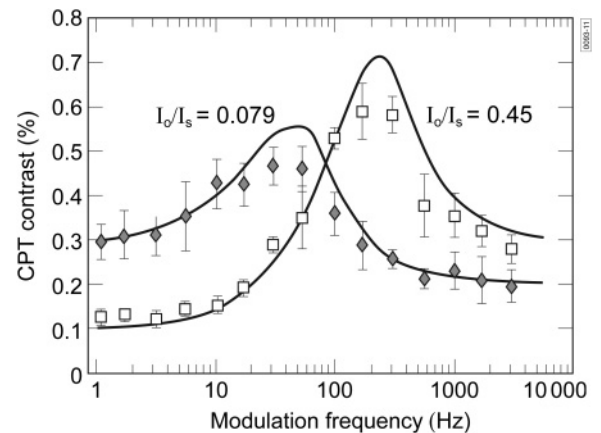

FIG. 6. The CPT contrast as a function of modulation frequency. Diamonds correspond to $I_o/I_s = 0.079$, the laser intensity that maximized our CPT contrast in the absence of polarization modulation, and the squares correspond to $I_o/I_s = 0.45$. The solid lines through the data correspond to the theory with $\gamma_1 = 63$ s^{-1}, and for $I_o/I_s = 0.079$ (i.e., $R = 251$ s^{-1}), we set $\gamma_2 = 723$ s^{-1}, while for $I_o/I_s = 0.45$ (i.e., $R = 1426$ s^{-1}), we set $\gamma_2 = 2640$ s^{-1}.

to the atom's quantization axis, the absorption cross section becomes

$$\sigma = \sigma_o \left\{ 1 - \xi \sum_{F,m} (-1)^{F-a} \frac{m}{2} \rho(Fm,Fm) \right.$$

$$\left. - 2\xi \, \mathrm{Re}[\rho(a0,b0)] \right\}, \tag{3}$$

where the $\rho(Fm,F'm')$ correspond to the alkali-metal ground-state density-matrix elements and we define the alkali-metal ground-state angular momentum quantum numbers F as $F = a \equiv I + \frac{1}{2}$ and $F = b \equiv I - \frac{1}{2}$, where, in these expressions, I is the alkali-metal nuclear spin. The change in the ground-state optical absorption cross section due to CPT comes from the last term in brackets on the right-hand side of Eq. (3), and we primarily focus on that term in what follows.

To highlight the important physical attributes of the problem, we now define $|b0\rangle$ as $|1\rangle$, $|a0\rangle$ as $|2\rangle$, and the $|5\,^2P_{1/2}\rangle$ multiplet of levels as $|3\rangle$. Thus, we reduce the full multilevel problem to the standard three-level Λ system for CPT. The multilevel nature of the problem and, in particular, the role of trapping states in the CPT problem [11] are included by normalizing the three-level system to η, the fractional ground-state population contributing to the CPT process (see the Appendix): $\rho_{11} + \rho_{22} + \rho_{33} = \eta$. Additionally, we assume that the sideband amplitudes are equal so that there is no hyperfine optical pumping: $\rho_{11} = \rho_{22}$.

With these assumptions, we transform to a rotating coordinate system [i.e., $\sigma_{mn} = \rho_{mn} e^{i\omega_{mn}t}$, where $\omega_{mn} = (E_m - E_n)/\hbar$] and make the rotating-wave approximation [27], thereby obtaining a system of density-matrix equations [28]. (Here, E_m and E_n are the energies of states $|m\rangle$ and $|n\rangle$, respectively),

$$\dot{\sigma}_{11} = -\Omega_{31} \mathrm{Im}[\sigma_{13} e^{-i\delta t}] + \frac{\Gamma}{2}(\eta - 2\sigma_{11}), \tag{4a}$$

$$\dot{\sigma}_{12} = -\frac{i}{2} e^{i\delta t}[\Omega_{32}\sigma_{13} + \Omega_{31}\sigma_{32}] - \gamma_2 \sigma_{12}, \tag{4b}$$

$$\dot{\sigma}_{13} = -\frac{i}{2}[\Omega_{32}\sigma_{12} e^{-i\delta t} - \Omega_{31} e^{i\delta t}(3\sigma_{11} - \eta)] - \frac{\Gamma}{2}\sigma_{13}, \tag{4c}$$

$$\dot{\sigma}_{23} = \frac{i}{2}[\Omega_{31}\sigma_{21} e^{i\delta t} - \Omega_{32} e^{-i\delta t}(3\sigma_{11} - \eta)] - \frac{\Gamma}{2}\sigma_{23}. \tag{4d}$$

In these expressions, Ω_{3j} is the Rabi frequency connecting $|j\rangle$ to $|3\rangle$, and in order to account for polarization modulation, we need to consider the effect of electric dipole coupling to the different excited-state Zeeman sublevels on the Rabi frequencies (i.e., $m_e = m_g + 1 \rightarrow m_e = m_g - 1$). First, though, we must attend to the definition of the Rabi frequency when the pressure broadening is greater than the excited-state hyperfine splitting.

Naively, since pressure broadening by the buffer gas washes out the excited-state hyperfine splitting in our experiments, one might be tempted to write the Rabi frequency as

$$\Omega_{3j} \sim \sum_{F_e} \langle F_e, \pm 1 | r_{1\xi} | F_g, 0 \rangle, \tag{5}$$

where $r_{1\xi}$ is a spherical tensor representing the electric dipole operator. However, Eq. (5) implies that the $|F_e, m_F\rangle$ basis functions are not eigenfunctions of the atomic Hamiltonian

and that the more appropriate eigenfunctions for calculating the Rabi frequency correspond to the set $|I, J_e, m_I, m_J\rangle$. Notice, though, that the cross section σ_B for N$_2$ collisions perturbing the 5 $^2P_{1/2}$ state is 3.3×10^{-14} cm^2 [19]. Thus, while the duration of a perturbing collision is $\sim 2\sqrt{\sigma_B/\pi}/\bar{v}$, the rate of perturbing collisions is $[N_{BG}]\bar{v}\sigma_B$, where $[N_{BG}]$ is the buffer-gas number density. Consequently, the fraction of time that the $|F_e, m_F\rangle$ basis functions are invalid (and, therefore, must be replaced by the $|I, J_e, m_I, m_J\rangle$ basis functions) is $\sim[N_{BG}]\sigma_B^{3/2}$. In our case, with 50 torr of N$_2$, this fraction is 10^{-2} so that most of the time the atoms' eigenfunctions correspond to the $|F_e, m_F\rangle$ basis set, and we should write

$$\Omega_{3j} \sim \langle F_e, \pm 1 | r_{1\xi} | F_g, 0 \rangle. \tag{6}$$

The fact that two excited-state hyperfine levels simultaneously connect to a single ground state simply implies that we have two subpopulations in our ensemble: those velocity subgroups interacting coherently through $|F_e = a\rangle$ and those velocity subgroups interacting coherently through $|F_e = b\rangle$.

Now, to proceed to the question of how laser polarization variations affect the Rabi frequency, from Eq. (6) and the Wigner-Eckart theorem (along with the expression for the reduced matrix element of a coupled system) [29], we have

$$\Omega_{3j} \sim (-1)^{F_e + F_g - a} \sqrt{(2F_g + 1)(2F_e + 1)}$$

$$\times \begin{pmatrix} F_e & 1 & F_g \\ -\xi & \xi & 0 \end{pmatrix} \begin{Bmatrix} \frac{1}{2} & F_e & I \\ F_g & \frac{1}{2} & 1 \end{Bmatrix} \langle 5\,^2P_{1/2} \| r \| 5\,^2S_{1/2} \rangle. \tag{7}$$

Note that this expression for Ω_{3j} is specific to the D_1 transition of the alkali metals and that the last term on the right-hand side of Eq. (7) is a reduced matrix element. Evaluating Ω_{3j} for ^{87}Rb (i.e., $I = 3/2$), we find for $F_e = b$ that

$$\Omega_{31} \sim \left(\frac{\xi}{2\sqrt{6}} \right) \langle 5\,^2P_{1/2} \| r \| 5\,^2S_{1/2} \rangle, \tag{8a}$$

$$\Omega_{32} \sim -\left(\frac{1}{2\sqrt{6}} \right) \langle 5\,^2P_{1/2} \| r \| 5\,^2S_{1/2} \rangle, \tag{8b}$$

while for $F_e = a$,

$$\Omega_{31} \sim \left(\frac{1}{2\sqrt{2}} \right) \langle 5\,^2P_{1/2} | r | 5\,^2S_{1/2} \rangle, \tag{8c}$$

$$\Omega_{32} \sim -\left(\frac{\xi}{2\sqrt{2}} \right) \langle 5\,^2P_{1/2} \| r \| 5\,^2S_{1/2} \rangle. \tag{8d}$$

Thus, when the polarization changes (i.e., $\xi \rightarrow -\xi$) only one of the Rabi frequencies in the Λ system changes sign. This is a key theoretical observation, without which, the splitting of the CPT resonance would not be predicted. Consequently, to include laser polarization modulation in the density-matrix equations, we let $\xi \rightarrow (e^{i\omega_m t} + e^{-i\omega_m t})/2$ and make the replacements,

$$\Omega_{31} \rightarrow \frac{\Omega_{31}}{2}(e^{i\omega_m t} + e^{-i\omega_m t}), \tag{9a}$$

$$\Omega_{32} \rightarrow \Omega_{32}. \tag{9b}$$

Substituting Eqs. (9) into Eqs. (4), and making an additional rotating coordinate-system transformation [30],

$$\tau_{12} = \sigma_{12} e^{-i(2\delta - \alpha\omega_m)t}, \tag{10a}$$

$$\tau_{13} = \sigma_{13} e^{-i(\delta - \alpha\omega_m)t}, \tag{10b}$$

$$\tau_{23} = \sigma_{23} e^{i\delta t}, \tag{10c}$$

where $\alpha \equiv \delta/|\delta|$, the density-matrix equations become

$$\dot{\sigma}_{11} = -\frac{\Omega_{31}}{2}\text{Im}[\tau_{13}(e^{i(1-\alpha)\omega_m t} + e^{-i(1+\alpha)\omega_m t})]$$
$$+ \frac{\Gamma}{2}(\eta - 2\sigma_{11}), \tag{11a}$$

$$\dot{\tau}_{12} = -\frac{i}{2}\left[\Omega_{32}\tau_{13} + \frac{\Omega_{31}}{2}\tau_{32}(e^{i(1+\alpha)\omega_m t} + e^{-i(1-\alpha)\omega_m t})\right]$$
$$- [\gamma_2 + i(2\delta - \alpha\omega_m)]\tau_{12}, \tag{11b}$$

$$\dot{\tau}_{13} = -\frac{i}{2}\left[\Omega_{32}\tau_{12} - \frac{\Omega_{31}}{2}(e^{i(1+\alpha)\omega_m t}\right.$$
$$\left. + e^{-i(1-\alpha)\omega_m t})(3\sigma_{11} - \eta)\right] - \left[\frac{\Gamma}{2} + i(\delta - \alpha\omega_m)\right]\tau_{13}, \tag{11c}$$

$$\dot{\tau}_{23} = \frac{i}{2}\left[\frac{\Omega_{31}}{2}\tau_{21}(e^{i(1+\alpha)\omega_m t} + e^{-i(1-\alpha)\omega_m t})\right.$$
$$\left. - \Omega_{32}(3\sigma_{11} - \eta)\right] - \left(\frac{\Gamma}{2} - i\delta\right)\tau_{23}. \tag{11d}$$

In Eqs. (11), one normally would proceed by making a secular approximation, arguing that, for a particular choice of δ, one of the oscillating coefficients in these equations becomes unity while the other quickly averages to zero (e.g., $\alpha \to +1$). This certainly is valid for large ω_m (i.e., $\omega_m \gg \gamma_2$) but unfortunately becomes problematic when ω_m is small. Specifically, while the oscillating coefficients can be replaced by unity for large ω_m, they should be replaced by 2 for $\omega_m \ll \gamma_2$. Since we are interested in exploring a full range of modulation frequencies, a naive application of the secular approximation to these equations is too limiting. Alternatively, retention of the oscillating coefficients makes an analytic solution impossible. Therefore, in the spirit of the secular approximation, we perform a filtered-response approximation for the oscillating coefficients,

$$(e^{i(1\pm\alpha)\omega_m t} + e^{-i(1\mp\alpha)\omega_m t}) \cong 1 + e^{\pm 2i\omega_m t} \to 1 + f_m, \tag{12a}$$

where we take

$$f_m = \frac{\gamma_m^n}{\sqrt{\gamma_m^{2n} + (2\omega_m)^{2n}}}. \tag{12b}$$

Briefly, we imagine that the atom's dephasing processes cause a filtering of the atom's response to the $2\omega_m$ oscillatory coefficients, and for the filtering function we choose an n-pole Butterworth filter [31] with cutoff frequency γ_m. (Obviously, other filtering functions could be chosen, and in future theoretical papers it may prove useful to compare and contrast the alternatives.) In what follows, we take $n = 1$ and $\gamma_m = \Omega^2/\Gamma + \gamma_2$. Although arguably crude, this approximation, nevertheless, has all the right characteristics: in the limit that ω_m is large, $1 + f_m \to 1$; in the limit that ω_m is small, $1 + f_m \to 2$, and the definition of large and small depends on

the modulation frequency's relationship to the 0-0 coherence's dephasing rate. Equations (11), therefore, become

$$\dot{\sigma}_{11} = -\frac{\Omega_{31}}{2}(1 + f_m)\text{Im}[\tau_{13}] + \frac{\Gamma}{2}(\eta - 2\sigma_{11}), \tag{13a}$$

$$\dot{\tau}_{12} = -\frac{i}{2}\left[\Omega_{32}\tau_{13} + \frac{\Omega_{31}}{2}\tau_{32}(1 + f_m)\right]$$
$$- [\gamma_2 + i(2\delta - \alpha\omega_m)]\tau_{12}, \tag{13b}$$

$$\dot{\tau}_{13} = -\frac{i}{2}\left[\Omega_{32}\tau_{12} - \frac{\Omega_{31}}{2}(1 + f_m)(3\sigma_{11} - \eta)\right]$$
$$- \left[\frac{\Gamma}{2} + i(\delta - \alpha\omega_m)\right]\tau_{13}, \tag{13c}$$

$$\dot{\tau}_{23} = \frac{i}{2}\left[\frac{\Omega_{31}}{2}(1 + f_m)\tau_{21} - \Omega_{32}(3\sigma_{11} - \eta)\right]$$
$$- \left(\frac{\Gamma}{2} - i\delta\right)\tau_{23}. \tag{13d}$$

To proceed, we first solve Eqs. (13c) and (13d) under the assumption that Γ is much larger than any other rate in the system so that, in effect, we approximate these density-matrix elements by their equilibrium values (i.e., $e^{-\Gamma t} \to 0$), obtaining

$$\bar{\tau}_{13} \cong -\frac{i}{\Gamma}\left[\Omega_{32}\tau_{12} - \frac{\Omega_{31}}{2}(1 + f_m)(3\sigma_{11} - \eta)\right], \tag{14a}$$

$$\bar{\tau}_{23} \cong \frac{i}{\Gamma}\left[\frac{\Omega_{31}}{2}(1 + f_m)\tau_{21} - \Omega_{32}(3\sigma_{11} - \eta)\right]. \tag{14b}$$

We then replace τ_{13} and τ_{23} in Eqs. (13a) and (13b) with their quasiequilibrium values [i.e., Eqs. (14)], take $|\Omega_{31}| = |\Omega_{32}| = \Omega$, and solve for τ_{12}, again recognizing that Γ is greater than any other rate in the system,

$$\text{Re}[\tau_{12}]$$
$$= \frac{2R\eta(1 + f_m)\{R[5 + f_m(2 + f_m)] + 8\gamma_2\}}{\{R[5 + f_m(2 + f_m)] + 8\gamma_2\}^2 + 64(2\delta - \alpha\omega_m)^2}, \tag{15a}$$

$$\text{Im}[\tau_{12}]$$
$$= -\frac{16R\eta(1 + f_m)(2\delta - \alpha\omega_m)}{\{R[5 + f_m(2 + f_m)] + 8\gamma_2\}^2 + 64(2\delta - \alpha\omega_m)^2}. \tag{15b}$$

Here, R, the photon absorption rate, is again defined as Ω^2/Γ. Then, from Eqs. (15), it is straightforward to show that

$$\text{Re}[\rho(a0,b0)] = A\sin[(\omega_{\text{hfs}} + 2\delta - \alpha\omega_m)t + \psi], \tag{16}$$

where

$$A = \frac{2R\eta(1 + f_m)}{\sqrt{\{R[5 + f_m(2 + f_m)] + 8\gamma_2\}^2 + 64(2\delta - \alpha\omega_m)^2}}, \tag{17a}$$

and

$$\psi = \tan^{-1}\left(\frac{\{R[5 + f_m(2 + f_m)] + 8\gamma_2\}}{8(2\delta - \alpha\omega_m)}\right). \tag{17b}$$

To calculate the transmitted light intensity, we employ Eq. (16) in Eq. (3) and follow Huang *et al.* [23] by recognizing that the modulated laser intensity mixes with the modulated

absorption cross section. As a consequence, the transmitted light intensity I_T is given by

$$I_T = I_c + 2I_s e^{-\kappa_o(1-2\overline{\langle S_z \rangle})}\{1 - \cos[\omega_{\text{hfs}} + 2\delta]t\}$$
$$\times \exp\{-2\kappa_o \cos(\omega_m t)A \sin[(\omega_{\text{hfs}} + 2\delta - \alpha\omega_m)t + \psi]\}. \tag{18}$$

For the modulation frequencies of interest (i.e., $\omega_m \ll \omega_{\text{hfs}}$), we can replace $\cos(\omega_m t)\sin[(\omega_{\text{hfs}} + 2\delta - \alpha\omega_m)t + \psi]$ by $\sin[(\omega_{\text{hfs}} + 2\delta)t + \psi]$. We then expand the second exponential in Eq. (18) and average over an intensity modulation period ω_o (i.e., $\omega_o \equiv \omega_{\text{hfs}} + 2\delta$),

$$I_T = I_c + 2I_s e^{-\kappa_o(1-2\overline{\langle S_z \rangle})} \sum_{n=0}^{\infty} \frac{(-2\kappa_o A)^n}{n!} \frac{\omega_o}{2\pi}$$
$$\times \int [1 - \cos(\omega_o t)]\sin^n(\omega_o t + \psi)dt. \tag{19}$$

Retaining terms of $(\kappa_o A)^2$ or lower, which represents a reasonably good approximation for the experimental conditions of most interest, Eq. (19) becomes

$$I_T \cong I_c + 2I_s e^{-\kappa_o(1-2\overline{\langle S_z \rangle})}\left(1 + \kappa_o A \sin\psi + \kappa_o^2 A^2\right), \tag{20}$$

so that the CPT resonance amplitude ΔI_{CPT} is given by

$$\Delta I_{\text{CPT}} = 2I_s e^{-\kappa_o(1-2\overline{\langle S_z \rangle})}\left(\kappa_o A \sin\psi + \kappa_o^2 A^2\right), \tag{21a}$$

and the CPT contrast becomes

$$\frac{\Delta I_{\text{CPT}}}{I_T} = \frac{2(I_s/I_c)e^{-\kappa_o(1-2\overline{\langle S_z \rangle})}\left(\kappa_o A \sin\psi + \kappa_o^2 A^2\right)}{1 + 2(I_s/I_c)e^{-\kappa_o(1-2\overline{\langle S_z \rangle})}}. \tag{21b}$$

Figure 7 shows the CPT line shapes predicted by Eq. (21a) for a number of modulation frequencies with $I_o/I_s = 0.45$ and $\gamma_2 = 320$ s^{-1} [see Fig. 3(b)], and as will be discussed in connection with Fig. 6, $\gamma_1 = 63$ s^{-1}. Clearly, the theory is qualitatively consistent with the experimental observations:

For modulation frequencies less than γ_1, the CPT line shape increases in amplitude; and for modulation frequencies greater than γ_2, the CPT line shape splits into a doublet with the doublet's resonant frequencies equal to $\pm\omega_m$. Furthermore, the amplitude of the CPT resonance reaches a maximum for $\omega_m \sim \gamma_2$.

Figure 6 shows a comparison between theory and experiment for the CPT contrast as a function of modulation frequency, allowing two free theoretical parameters: γ_1 and γ_2. We note, however, that γ_1 is constrained to be the same value for the two different light intensities. For the best fit in the two cases, we set $\gamma_1 = 63$ s^{-1} (consistent with the anticipated range of values for this parameter: 50–110 s^{-1}), and R is defined through its relation to I_o/I_s [see Fig. 3(b)]. Overall, the agreement between theory and experiment is very good with $\gamma_2 = 723$ s^{-1} for $I_o/I_s = 0.079$ and $\gamma_2 = 2640$ s^{-1} for $I_o/I_s = 0.45$, and we take this as fairly strong evidence that the theory captures the important physical processes generating the atomic dynamics in the presence of polarization modulation. It also, however, points out the most limiting feature of the analytical theory: The γ_2 we require to get good agreement for the CPT amplitudes is larger than the γ_2 we require to reproduce the CPT linewidths (i.e., Fig. 7), and γ_2 varies as a function of R. This limiting feature of the analytical theory, though, should not be too surprising. In making the filtered-response approximation [i.e., Eq. (12a) *with the specific choice of* $n = 1$], we have called on γ_2 to perform double duty: It must describe the random dephasing of the ensemble, and it must act as a bridge between the secular approximation (i.e., $\omega_m \to \infty$) and the quasistatic approximation (i.e., $\omega_m \to 0$). Consequently, we might have anticipated that this single parameter would have difficulty accomplishing both tasks. In future experimental and theoretical work, it will prove enlightening to more fully explore the filter-response approximation, and to better understand the relationship between γ_m and γ_2 in the approximation.
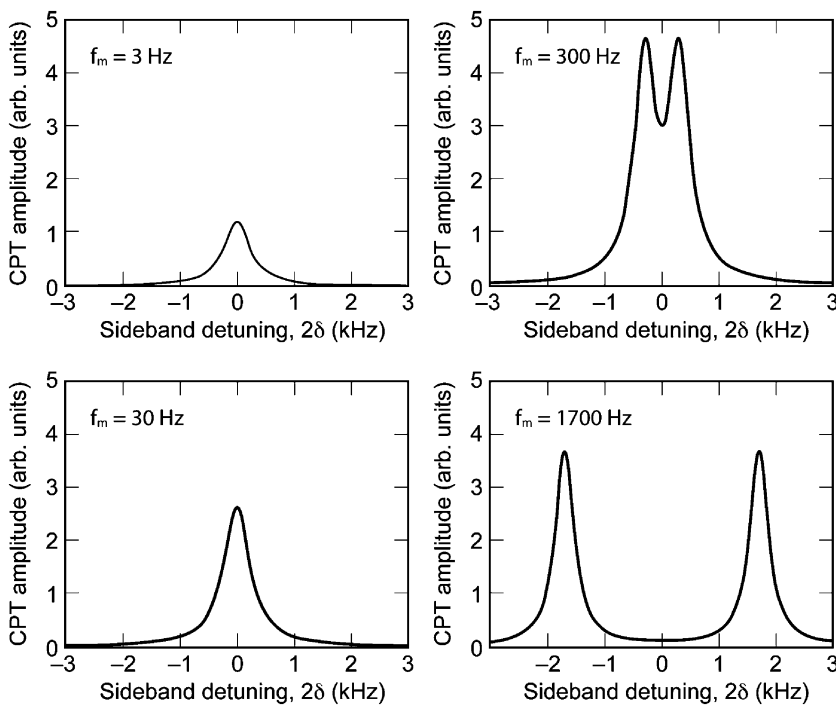

FIG. 7. Theoretical CPT line shapes under polarization modulation. Similar to the experimental findings, we see that for $\omega_m < \gamma_1$, the CPT amplitude increases with modulation frequency. Furthermore, when $\omega_m > \gamma_2$, the CPT resonance splits into a doublet, whose amplitude decreases with increasing modulation frequency.

IV. DISCUSSION

As noted in Sec. I, one of our primary motivations for studying the effects of polarization modulation on CPT signals was to better understand the manner in which stochastic processes enter and influence atomic dynamics; recognizing that polarization fluctuations may appear in a Λ system as a consequence of microphonics or through the use of VCSEL diode lasers [32]. The present paper shows that not only will stochastic polarization fluctuations add noise N to a CPT signal, but also the fluctuations will likely affect the CPT signal amplitude S and quality factor Q. In other words, with the performance of atomic clocks and atomic magnetometers defined by $Q(S/N)$, polarization fluctuations will affect the performance of such devices through all three parameters.

In order to gain some sense of how large the effects on the product SQ might be, we first note that it is possible to interpret the power spectrum of a stochastic process $L(\omega_m)$ in terms of the likelihood of a Fourier component of the random process appearing in a long-time history of the process. Thus, $L(\omega_m)d\omega_m$ can be taken as the probability that a random process will exhibit Fourier components ranging from $\omega_m - d\omega_m/2$ to $\omega_m + d\omega_m/2$. Furthermore, if we ignore the transients induced in the atomic system when the rate of polarization fluctuations changes (i.e., when $\omega_m \rightarrow \omega_m + d\omega_m$), then we can make a simple application of the ergodic theorem in order to write averages over time in terms of ensemble averages over ω_m. This latter approximation is valid if the correlation time of the stochastic process τ_c is much longer than the dephasing time of the atomic system but certainly becomes problematic as the correlation time shortens. Nevertheless, this approximation should be workable for our present purposes since we are only interested in gaining an illustrative understanding of stochastic-field effects in the atomic linewidth regimes of most interest. Consequently, we write the CPT line shape in the presence of polarization fluctuations very roughly as

$$\Delta I_{\text{CPT}} \sim 2I_s e^{-\kappa_o(1-2\overline{\langle S_z \rangle})}$$
$$\times \int_{-\infty}^{\infty} L(\omega_m)\big(\kappa_o A \sin\psi + \kappa_o^2 A^2\big)d\omega_m. \quad (22)$$
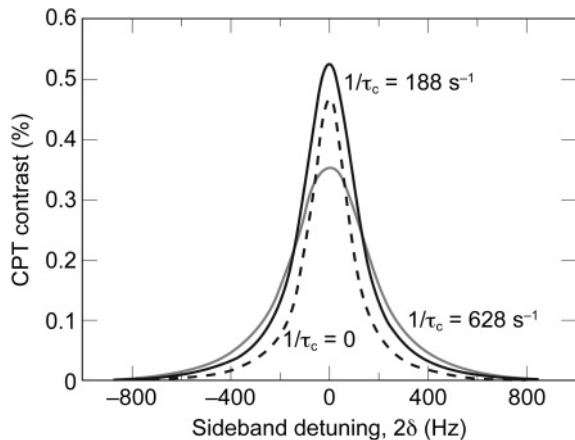
FIG. 8. Illustrative prediction of the CPT contrast as a function of sideband detuning for several values of a broadband stochastic-field's correlation time for polarization fluctuations.
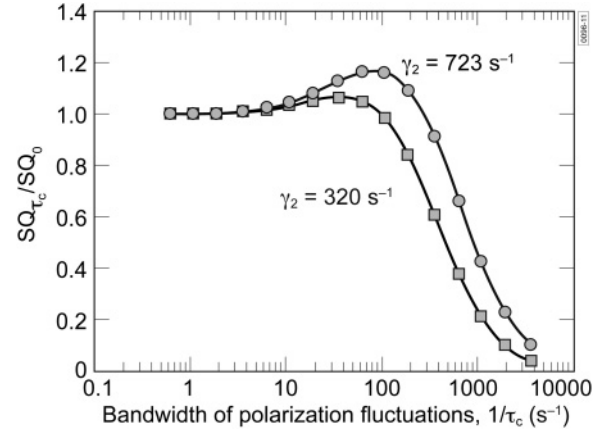
FIG. 9. Illustrative prediction of the relative change in the product SQ as a function of the correlation time for laser polarization fluctuations: Squares correspond to $\gamma_2 = 320$ s^{-1}, our measured dephasing rate, while circles correspond to $\gamma_2 = 723$ s^{-1}, the dephasing rate giving good experimental-theoretical agreement, in Fig. 6, for $I_o/I_s = 0.079$.

Taking the power spectrum as a Lorentzian with correlation time τ_c,

$$L(\omega_m) = \frac{\tau_c/\pi}{1 + (\omega_m \tau_c)^2}, \quad (23)$$

Figure 8 shows several examples of the CPT line shape for various values of τ_c, with $\gamma_1 = 63$, $\gamma_2 = 320$, and $R = 251$ s^{-1} (i.e., $I_o/I_s = 0.079$, the light intensity that maximized the CPT contrast). Clearly, as the correlation time shortens, the CPT line shape decreases in amplitude and broadens as fast Fourier components in the power spectrum of the polarization fluctuations lead to CPT doublets. Figure 9 shows the product SQ found through Eq. (22) (i.e., $SQ_{\tau c}$) normalized to its value in the absence of polarization fluctuations (i.e., SQ_0). Here, we see that, for $(R + \gamma_2)\tau_c \sim 10$, there is a slight increase in SQ as polarization fluctuations reduce the density of atoms in the trapping state, but then, the product decreases for shorter values of τ_c since fast Fourier components in the stochastic process lead to a CPT doublet splitting and, hence, a reduction in Q.

Obviously, given the approximations in obtaining Figs. 8 and 9, the results should be taken as illustrative and, at best, semiquantitative. Nevertheless, they do capture the significance of the problem: Broadband polarization fluctuations in Λ systems can have a significant effect on CPT signals and observed linewidths. In the future, we plan to examine the full stochastic-field problem by introducing broadband polarization noise into a CPT system and measuring SQ/N. The results from that work should give experimenters a better idea of how well they need to understand the magnitude and origins of polarization noise in their basic and applied physics experiments.

program, funded by the US Air Force Space and Missile Systems Center under Contract No. FA8802-09-C-0001.

APPENDIX: ELECTRON-SPIN POLARIZATION MODULATION

As noted in the main text, laser polarization modulation has two effects on a CPT signal: It modulates the coherence, which is the source of CPT, and it modulates the population density in trapping states, parametrized in the case of the alkali metals by $\langle S_z \rangle$, the average alkali-metal electron-spin polarization in the ground state. While, in general, these two effects are coupled (i.e., variations in the 0-0 coherence drive variations in $\langle S_z \rangle$, and variations in $\langle S_z \rangle$ affect the number of atoms participating in the 0-0 coherence), our theory separates the two. Thus, we consider the effect of polarization modulation on $\langle S_z \rangle$ in the absence of coherence, and we then employ the average value of $\langle S_z \rangle$ over a modulation half cycle to account for the fractional population of atoms participating in the 0-0 coherence. In this Appendix, we consider the first of these problems (i.e., the determination of the average value of $\langle S_z \rangle$ during modulation).

For vapor-phase atoms described by a density matrix ρ, $\langle S_z \rangle$ equals $\mathrm{Tr}[\rho S_z]$ [29] and to compute the temporal variation of $\langle S_z \rangle$ under polarization modulation, we will assume uniform relaxation of the ground-state Zeeman sublevels [33]. While this is a fair assumption in situations where relaxation is dominated by diffusion, in our experiments relaxation more likely proceeds though electron randomization arising from Rb/N_2 collisions [23]. Nevertheless, at the present theory's level of approximation, the assumption of uniform relaxation is reasonable, and with it the analysis is greatly simplified. Consequently, ignoring repopulation pumping [8] due to the relatively high buffer-gas pressure in our experiments, and the concomitant fast rate of excited-state depolarization and

quenching [34], we have

$$\langle \dot{S}_z \rangle = -\left(\frac{\Omega^2}{\Gamma} + \gamma_1\right) S_z + \frac{\xi \Omega^2}{2\Gamma}, \qquad (A1)$$

where Ω is the optical Rabi frequency, Γ is the $5\,^2P_{1/2}$ decay rate, γ_1 is the (longitudinal) uniform relaxation rate among the ground-state Zeeman sublevels, and ξ is the circularly polarized photon's spin (i.e., $s_+ \Rightarrow \xi = +1$ and $s_- \Rightarrow \xi = -1$). Solving Eq. (A1), we obtain

$$\langle S_z \rangle = \frac{\xi R}{2(R + \gamma_1)} + B e^{-(R+\gamma_1)t}, \qquad (A2)$$

where R is defined as Ω^2/Γ and is equal to the photon-absorption rate.

To determine B, we note that for square-wave polarization modulation, if the laser switches between circular polarization states at the rate $2/T_m$, where T_m is the modulation period, then $\langle S_z(t=0)\rangle = -\langle S_z(t=T_m/2)\rangle$. With this as the initial condition, we then find that

$$\langle S_z \rangle = \left(\frac{\xi R}{R + \gamma_1}\right)\left(\frac{1}{2} - \frac{e^{-(R+\gamma_1)t}}{1 + e^{-(R+\gamma_1)T_m/2}}\right). \qquad (A3)$$

Averaging $\langle S_z \rangle$ over a half-modulation cycle then yields

$$\overline{\langle S_z \rangle} = \frac{1}{2}\left(\frac{\xi R}{R + \gamma_1}\right)\left[1 - \frac{2}{\pi}\left(\frac{\omega_m}{R + \gamma_1}\right)\tanh\left(\frac{\pi(R+\gamma_1)}{2\omega_m}\right)\right]. \qquad (A4)$$

For an alkali-metal atom with nuclear spin I, the fraction of ground-state atoms contributing to the 0-0 ground-state coherence η can be written approximately as

$$\eta = \frac{1}{2I+1}(1 - 2\vec{s} \cdot \langle \vec{S} \rangle), \qquad (A5)$$

where $\vec{s}$ is the photon spin with eigenvalue ξ. For present purposes, where the photon spin is either parallel or antiparallel to the atom's quantization axis, we have $\eta = (1 - 2|\langle S_z \rangle|)/(2I+1)$.

[1] G. Alzetta, A. Gozzini, L. Moi, and G. Orriols, Nuovo Cimento Soc. Ital. Fis., B **36B**, 5 (1976).

[2] E. Arimondo and G. Orriols, Lett. Nuovo Cimento Soc. Ital. Fis. **17**, 333 (1976).

[3] S. Knappe, V. Shah, P. D. D. Schwindt, L. Hollberg, J. Kitching, L.-A. Liew, and J. Moreland, Appl. Phys. Lett. **85**, 1460 (2004).

[4] R. Lutwak, J. Deng, W. Riley, M. Varghese, J. Leblanc, G. Tepolt, M. Mescher, D. K. Serkland, K. M. Geib, and G. M. Peake, in *Proceedings of the 36th Annual Precise Time and Time Interval (PTTI) Systems and Applications Meeting* (US Naval Observatory, Washington, DC, 2004), pp. 339–354.

[5] M. O. Scully and M. S. Zubairy, *Quantum Optics* (Cambridge University Press, Cambridge, UK, 1997), Chap. 7.

[6] A. B. Post, Y.-Y. Jau, N. N. Kuzma, and W. Happer, Phys. Rev. A **72**, 033417 (2005).

[7] F. Levi, A. Godone, J. Vanier, S. Micalizio, and G. Modugno, Eur. Phys. J. D **12**, 53 (2000).

[8] W. Happer, Rev. Mod. Phys. **44**, 169 (1972).

[9] L. C. Balling, in *Advances in Quantum Electronics*, edited by D. W. Goodwin (Academic, London, 1975), Vol. 3, pp. 1–167.

[10] W. Happer and W. A. Van Wijngaarden, Hyperfine Interact. **38**, 435 (1987).

[11] J. Vanier, M. W. Levine, D. Janssen, and M. Delaney, Phys. Rev. A **67**, 065801 (2003).

[12] Y.-Y. Jau, E. Miron, A. B. Post, N. N. Kuzma, and W. Happer, Phys. Rev. Lett. **93**, 160802 (2004).

[13] T. Zanon, S. Guerandel, E. de Clercq, D. Holleville, N. Dimarcq, and A. Clairon, Phys. Rev. Lett. **94**, 193002 (2005).

[14] M. Rosenbluh, V. Shah, S. Knappe, and J. Kitching, Opt. Express **14**, 6588 (2006).

[15] V. Shah, S. Knappe, P. D. D. Schwindt, V. Gerginov, and J. Kitching, Opt. Lett. **31**, 2335 (2006).

[16] J. Camparo, in *Proceedings of the 7th Symposium Frequency Standards and Metrology*, edited by L. Maleki (World Scientific, Hackensack, NJ, 2009), pp. 109–117.

[17] J. Camparo, Contemp. Phys. **25**, 443 (1985).

[18] J. Kaiser, C. Degen, and W. Elsässer, J. Opt. Soc. Am. B **19**, 672 (2002).

[19] M. D. Rotondaro and G. P. Perram, J. Quant. Spectrosc. Radiat. Transf. **57**, 497 (1997).

[20] J. H. Moore, C. C. Davis, and M. A. Coplan, *Building Scientific Apparatus* (Addison-Wesley, London, 1983), Chap. 5.

[21] M. S. Safronova and U. I. Safronova, Phys. Rev. A **83**, 052508 (2011).

[22] E. S. Hrycyshyn and L. Krause, Can. J. Phys. **48**, 2761 (1970).

[23] M. Huang, J. G. Coffer, and J. C. Camparo, J. Phys. B **43**, 135001 (2010).

[24] S. Goldman, *Frequency Analysis, Modulation and Noise* (McGraw-Hill, New York, 1948), Chap. 7.

[25] A. Shevchenko, M. Kaivola, and J. Javanainen, Phys. Rev. A **73**, 035801 (2006).

[26] W. Happer, Y.-Y. Jau, and T. Walker, *Optically Pumped Atoms* (Wiley-VCH, Weinheim, 2010), Chap. 6.

[27] L. Allen and J. H. Eberly, *Optical Resonance and Two-Level Atoms* (Dover, New York, 1975); M. O. Scully and M. S. Zubairy, *Quantum Optics* (Cambridge University Press, Cambridge, UK, 1997); C. C. Gerry and P. L. Knight, *Introductory Quantum Optics* (Cambridge University Press, Cambridge, UK, 2005).

[28] Normally, in the density-matrix equations, there should be a longitudinal relaxation term for σ_{11}: $\gamma_1(\sigma_{22} - \sigma_{11})$. However, with our assumption that $\sigma_{22} = \sigma_{11}$, longitudinal relaxation plays no role in these density-matrix equations.

[29] K. Blum, *Density Matrix Theory and Applications* (Plenum, New York, 1981).

[30] In Eqs. (4), we transformed the equations into a coordinate system rotating at the atom's resonant frequency. However, in this coordinate system the field still appears to be oscillating since the field is detuned from resonance. In the transformation embodied by Eqs. (10), we compensate for the residual oscillation of the field due to its detuning by transforming into a coordinate system where one component of the oscillating field appears to be stationary. Obviously, we could have performed a single rotating coordinate transformation at the outset to arrive at Eqs. (10). However, we felt that it was important to illuminate the fact that, even with careful consideration of rotating coordinate system transformations, polarization modulation, nonetheless, leaves an oscillating term in the equations that cannot be ignored via the standard rotating-wave approximation.

[31] P. Horowitz and W. Hill, *The Art of Electronics* (Cambridge University Press, Cambridge, UK, 1989), Chap. 5.

[32] J. Kaiser, C. Degen, W. Elsässer, J. Opt. Soc. Am. B **19**, 672 (2002).

[33] F. A. Franz, Phys. Rev. **141**, 105 (1966).

[34] A. Sieradzan and F. A. Franz, Phys. Rev. A **25**, 2985 (1982).